

# Drift and Diffusion of Spins Generated by the Spin Hall Effect

N. P. Stern, D. W. Steuerman, S. Mack, A. C. Gossard, and D. D. Awschalom\*

*Center for Spintronics and Quantum Computation,  
University of California, Santa Barbara, CA 93106 USA*

(Dated: February 4, 2008)

## Abstract

Electrically generated spin accumulation due to the spin Hall effect is imaged in  $n$ -GaAs channels using Kerr rotation microscopy, focusing on its spatial distribution and time-averaged behavior in a magnetic field. Spatially-resolved imaging reveals that spin accumulation observed in transverse arms develops due to longitudinal drift of spin polarization produced at the sample boundaries. One- and two-dimensional drift-diffusion modeling is used to explain these features, providing a more complete understanding of observations of spin accumulation and the spin Hall effect.

The observation of current induced spin polarization<sup>1</sup> and the spin Hall effect<sup>2</sup> demonstrate all-electrical generation of spin polarization through the spin-orbit interaction. A detailed understanding of spin accumulation produced by these phenomena is a prerequisite to advancing spin-based electronics applications. Sample boundaries in spin-orbit systems are an active topic of research, affecting both the observed spin accumulation near and away from sample edges<sup>3</sup> and even the proper theoretical definition of a spin current<sup>4</sup>. For spin Hall systems in the extrinsic regime, many of these complications can potentially be avoided because the spin-orbit coupling is weak, enabling simple solutions to spin diffusion equations<sup>5</sup> which have been used to explain spin accumulation in a number of studies<sup>2,3,6,7</sup>.

Despite these expected simplifications in the analysis of the extrinsic spin Hall effect, spatially-resolved optical measurements have revealed spin accumulation which is not entirely explained by simple one-dimensional spin diffusion models<sup>2,3</sup>. In this Letter we measure spin accumulation with unambiguous contributions from both drift along electric fields and spin precession about an applied magnetic field. We develop a diffusion model in one- and two-dimensions which can reproduce the observations as well as allow reinterpretation of the details of recent experiments on the spin Hall effect. These results provide a more complete understanding of the behavior of electrically generated spin polarization in micron-scale devices.

The structures discussed in this manuscript are fabricated from a 2- $\mu\text{m}$  thick epilayer of  $n\text{-GaAs}$  deposited on 200 nm of undoped  $\text{Al}_{0.4}\text{Ga}_{0.6}\text{As}$  grown by molecular beam epitaxy. The  $n\text{-GaAs}$  is Si-doped with  $n = 3 \times 10^{16} \text{ cm}^{-3}$  (at 30 K) for long spin coherence times as in Ref. 2. Using standard photolithography and wet etching, the  $n\text{-GaAs}$  is patterned into 300- $\mu\text{m}$  long, 60- $\mu\text{m}$  wide channels with a 60- $\mu\text{m}$  long, 30- $\mu\text{m}$  wide transverse arm (Fig. 1a). The  $n\text{-GaAs}$  is contacted by annealed  $\text{Au/Ni/Au/Ge/Ni}$ . The devices are mounted in a helium flow cryostat with the channel defined to be the  $x$  direction and a magnetic field  $B$  applied in the  $y$  direction. All measurements reported are at 30 K, and have been repeated in a variety of similar  $n\text{-GaAs}$  wafers and channels of various dimensions. An AC square voltage with frequency  $f_V = 1.168 \text{ kHz}$  is applied across the device, driving a current in the  $\pm x$  direction and generating spin polarization  $s^z$  in the  $\pm z$  direction due to the spin Hall effect<sup>2</sup>.

Spin accumulation is measured using a Kerr rotation microscope with a spatial resolution of  $\sim 1 \mu\text{m}$ <sup>8</sup>. A linearly polarized beam from a pulsed Ti:sapphire laser tuned to  $\lambda = 821 \text{ nm}$

is focused through a microscope objective normal to the sample surface and the polarization of the reflected beam is analyzed with a balanced photodiode bridge and lock-in amplifier operating at  $f_V$ . The axis of linear polarization rotates by an angle  $\theta_K$  proportional to  $s^z$  due to the Kerr effect. The microscope objective is scanned over the device to spatially map  $s^z$  while using the reflectivity of the laser over the channel edges to calibrate the coordinate position.

Spatial profiles across the channel width (Fig. 1b) show a hyperbolic sine form for  $s^z(y)$ , as expected from solution of basic diffusion equations<sup>2,5</sup>. Spin accumulation in the channel is measured at least a few spin diffusion lengths ( $L_s \sim 5\mu\text{m}$ ) away from the arm edge to minimize diffusive effects from the transverse arm. Sweeps of  $B$  produce a quasi-Lorentzian lineshape due to the time-averaged projection of  $s^z$  known as the Hanle effect<sup>2</sup>(Fig. 1c). The spin coherence time can be extracted from the half-width  $B_{1/2}$  of a Lorentzian fit to the magnetic field scans,  $\tau = \hbar/g\mu_B B_{1/2}$ , where  $\hbar$  is the reduced Planck's constant,  $g = -0.44$  is the g factor for GaAs, and  $\mu_B$  is the Bohr magneton.  $\tau$  decreases with increasing applied  $E$ , which has been previously explained as increased D'yakonov-Perel spin scattering due to electron heating<sup>9</sup>. As a function of  $y$ , the central peak narrows away from the channel edge, causing an apparent increase in the extracted  $\tau$  toward the center of the channel (Fig. 1b inset). This feature is consistent with previous observations of the spin Hall effect<sup>2,7</sup>. Increased averaging in the current measurements also reveals that  $s^z$  changes sign away from the central peak. Similarly, magnetic field scans in the transverse arm are more complicated than those in the main channel, exhibiting sign reversals and narrow central peaks (Fig. 1d) that cannot be fit by a Lorentzian lineshape. The cause of the departures from simple Lorentzian behavior in both the channel and the arms is expected to be due to a combination of spin precession, drift, and diffusion<sup>3</sup>, but detailed calculations of both the spatial and  $B$  dependences of the experimental data have so far been lacking. The remainder of this Letter will present modeling necessary to understand the above observations of spin accumulation due to the spin Hall effect.

In order to model spin accumulation, we assume that spin is generally conserved except for a decay with time constant  $\tau$ . The sample boundaries are treated as hard walls; neither charge nor spin can penetrate sample edges, and the edge causes no spin-orbit induced spin-flips. These approximations are both reasonable as GaAs is expected to be in the extrinsic limit of the SHE where spin-orbit coupling is weak. Under these assumptions, the vector

spin density  $s^i$  obeys a steady state continuity equation with additional spin precession and decay terms:

$$\frac{ds^i}{dt} = -\nabla \cdot \vec{J}_s^i - \frac{s^i}{\tau} + (\vec{\omega} \times \vec{s})^i = 0 \quad (1)$$

where  $\vec{\omega} = g\mu_B B / \hbar$  is the Larmor frequency vector and  $\vec{J}_s^i$  is the spin current of the  $i$ -th component of spin, which is defined in the simplest fashion as a sum over all particles of the product of spin and velocity:  $\vec{J}_s^i = \sum s^i \vec{v}$ . A general treatment using a more complicated definition of spin current<sup>4</sup>, which is potentially necessary in the intrinsic regime, is not necessary in this case. For electrons with isotropic, spin-independent transport properties, the spin current tensor is:

$$J_{s,j}^i = -\mu s^i E_j - D \partial_j s^i + \sigma_{SH} \epsilon^{ijk} E_k \quad (2)$$

where  $\mu$  is the charge mobility,  $\vec{E}$  the electric field,  $D$  the diffusion constant,  $\sigma_{SH}$  the spin Hall conductivity, and  $\epsilon^{ijk}$  the antisymmetric symbol. The first term represents drift of spin polarized carriers along the electric field, the second term governs diffusion of accumulated spin polarization, and the third is the spin current generated transverse to an electric field by the spin Hall effect.

Spin and charge coupling<sup>5</sup> is assumed to be negligible for simplicity, decoupling the electric field solution from the spin accumulation. This additional coupling does not appear to be necessary to capture the salient features of the experimental observations. Introducing the spin diffusion length  $L_s = \sqrt{D\tau}$ , the drift-diffusion equation in the channel is obtained from Eq. 1 and Eq. 2:

$$\partial^2 s^i + \frac{\mu\tau}{L_s^2} E_j \partial_j s^i - \frac{s^i}{L_s} + \frac{\tau\vec{\omega}}{L_s^2} \times \vec{s} = 0 \quad (3)$$

In Eq. 3, we assume the system is in the linear transport regime, where  $\sigma_{SH}$  is independent of electric field and the electron density is uniform. Because the electric field has no curl, the divergence of the spin Hall current is identically zero:  $\partial_j (\sigma_{SH} \epsilon^{ijk} \vec{E}_k) = \sigma_{SH} (\epsilon^{ijk} \partial_j E_k) = 0$ . For linear transport, the spin Hall current does not act as a source for spin accumulation in bulk; all spin accumulation arises from boundary accumulation at the channel edge. Recent modeling<sup>11</sup> has shown that bulk spin accumulation can indeed occur in a non-linear transport regime where the divergence of the spin Hall current is not identically zero; we do not study this effect in this manuscript. Eq. 3 represents a system of coupled linear differential equations for  $s^i$  written entirely in terms of experimentally determined parameters.

These equations include drift and spin precession terms, both of which have demonstrable consequences in the experimental data presented in Fig. 1.

In the case of an infinitely long channel oriented along the  $x$  direction (which is applicable far from the contacts and transverse arms),  $s^i$  will be independent of  $x$  and the local electric field will be a constant  $\vec{E} = E\hat{x}$ , causing the drift term to vanish and validating the assumption  $\sigma_{SH}(E) = \sigma_{SH}$  of Eq. 3. Specializing to the case of  $B$  along  $y$ , Eq. 3 reduces to two non-trivial coupled differential equations for  $s^x(y)$  and  $s^z(y)$ , which can be solved exactly by enforcing the boundary condition  $\hat{n} \cdot \vec{J}_s^i = 0$ . These diffusion equations including spin precession were solved for the case of spin accumulation in a one-dimensional system with polarized spins injected from ferromagnetic contacts<sup>13</sup>. The difference in this case is that the spin polarization is generated at the channel edge by the spin Hall effect. The spatial profile  $s^z(y)$  at  $B = 0$  is the same hyperbolic sine solution used in earlier analysis of the SHE<sup>5?</sup>. Near the channel edge,  $s^z(B)$  has the expected Lorentzian shape from the Hanle model. Away from the channel edge, spin precession modifies the steady state solution  $s^z(B)$ , resulting in a narrowing central peak and oscillations in the tails. Calculations of the  $s^z(B)$  dependence are shown in Fig. 2a, assuming  $\tau = 2.5$  ns and  $L_s = 4.5\mu\text{m}$ , overlaid with the normalized data from Fig. 1b. The narrowing of the central peak and the sign change of  $s^z$  are evident both in these  $B$  scans and in the full  $B$  and  $y$  dependence of the data and calculations in Fig. 2c. Within the diffusion model, the central peak narrowing and the non-Lorentzian tails of Fig. 1c can be entirely understood as spin precession of diffusing spins with a constant  $\tau$  without invoking a position-dependent spin coherence time.

We apply the model discussed above to two-dimensional geometries as well, focusing on the transverse arm originally investigated by Sih et al.<sup>3</sup> In this geometry, the drift term of the equations plays an important role. Two-dimensional finite element modeling is used to first solve for the electric field  $\vec{E}(x, y)$  and then use Eqs. 1 and 2 to find the magnitude of spin polarization  $s^z(x, y)$ . As before, we fix  $L_s = \sqrt{D\tau}$  to be equal to that measured from magnetic field scans along  $y$  in Fig. 1b. Since the magnitude of the electric field,  $E$ , varies throughout the sample, we use in the model the  $\tau(E)$  and  $\mu(E)$  measured separately for this sample. We note that good agreement with the data is also observed by fixing  $\tau$  and  $\mu$  to their  $E = 0$  values, with the reduced mobility being countered by the factor of five increase in  $\tau$ . The results we present here use the measured  $\tau(E)$  and  $\mu(E)$ , however, as this more likely describes the true dynamics of the mobile electron spins. The model accounts for both

the  $B = 0$  spatial profile and the field dependence observed in linecuts at  $x = 0$  (Fig. 2d). Contrary to the model in Ref. 3, this model does not require electron spins to have a drift velocity transverse to the electron current.

In order to confirm the effects of drift in accumulation from the spin Hall effect, we obtain two-dimensional maps of spin polarization in the transverse arm by modulating the magnetic field at  $f_B = 3.3$  Hz and detecting the resulting Kerr rotation with lockin amplifiers at  $f_V \pm 2f_B$ . The resulting signal will be proportional to the second derivative of the magnetic field profile near  $B = 0$ ? Kato:2004b), allowing efficient two-dimensional imaging of spin accumulation without time-consuming magnetic field scans. Fig. 3a shows an image of KR in the 60- $\mu\text{m}$  long transverse arm extending from a 300- $\mu\text{m}$  long channel. Spin accumulation is observed across the entire width of the arm, extending 40  $\mu\text{m}$  from the main channel, as observed in Ref. 3. This measurement is performed with a symmetric square wave current, so the observed accumulation is symmetric about the center of the arm at  $x = 0$  (Fig. 3a). Conclusive evidence of the importance of drift in the spin accumulation is obtained by applying an AC voltage with a DC offset to create a square wave electric field between 0 mV/ $\mu\text{m}$  and  $E$ . This slight modification allows the lock-in detection technique to remain unchanged, but removes the symmetric current flow so that electrons only flow in one general direction along the channel. Figs. 3b and 3c show the data and model for the spin accumulation in the transverse arm under unidirectional current flow. The accumulation profile in the transverse arm is asymmetric about the arm center, and reverses direction when the current direction is reversed. The spin polarization observed in the transverse arm is neither generated in the arm itself, nor does it come from the spin Hall current generated in the bulk of the channel; it consists primarily of spin polarization sourced near the channel edge that travels longitudinally along the electric field lines that penetrate into the arm. These results accentuate the importance of including spin drift along the electric field in analysis of both one- and two-dimensional spin accumulation profiles.

In conclusion, we have provided experimental evidence that, in addition to diffusion, drift and spin precession are important factors in understanding the spin polarization generated by the spin Hall effect. Spatial profiles of spin accumulation and its evolution in an external magnetic field can be predicted by drift-diffusion modeling independently of any detailed treatment of the microscopic physics of the spin Hall effect. The practical ability to accurately model spin accumulation generated from the spin Hall effect enables reliable

engineering of electrically-generated spin accumulation profiles in devices.

We thank NSF and ONR for financial support. N. P. S. acknowledges the support of the Fannie and John Hertz Foundation, and S.M. acknowledges the NDSEG Fellowship. We gratefully thank J. Heron for his assistance with transport measurements.

---

\* Electronic address: awsch@physics.ucsb.edu

- <sup>1</sup> Y. Kato, R. C. Myers, A. C. Gossard, and D. D. Awschalom, Phys. Rev. Lett. **93**, 176601 (2004).
- <sup>2</sup> Y. Kato, R. C. Myers, A. C. Gossard, and D. D. Awschalom, Science **306**, 1910 (2004).
- <sup>3</sup> V. Sih, W. H. Lau, R. C. Myers, V. R. Horowitz, A. C. Gossard, and D. D. Awschalom, Phys. Rev. Lett. **97**, 096605 (2006).
- <sup>4</sup> J. Shi, P. Zhang, D. Xiao, and Q. Niu, Phys. Rev. Lett. **96**, 076604 (2006).
- <sup>5</sup> W-K. Tse, J. Fabian, I. Žutić, and S. Das Sarma, Phys. Rev. B **72**, 241303(R) (2005).
- <sup>6</sup> S. O. Valenzuela and M. Tinkham, Nature **442**, 176 (2006).
- <sup>7</sup> N. P. Stern, S. Ghosh, G. Xiang, M. Zhu, N. Samarth and D. D. Awschalom, Phys. Rev. Lett. **97**, 126603 (2006).
- <sup>8</sup> J. Stephens, R. K. Kawakami, J. Berezovsky, M. Hanson, D. P. Shepherd, A. C. Gossard, and D. D. Awschalom, Phys. Rev. B **68**, 041307(R) (2003).
- <sup>9</sup> M. Beck, C. Metzner, S. Malzer, and G. H. Döhler, Europhys. Lett. **75**, 597 (2006).
- <sup>10</sup> H-A. Engel, B. I. Halperin, and E. I. Rashba, Phys. Rev. Lett. **95**, 166605 (2005).
- <sup>11</sup> I. Finkler, H-A Engel, E. I. Rashba, and B. I. Halperin, cond-mat/0703654.
- <sup>12</sup> E. I. Rashba, Physica E **34**, 31 (2006).
- <sup>13</sup> M. Johnson and R. H. Silsbee, Phys. Rev. B **37**, 5312 (1988).

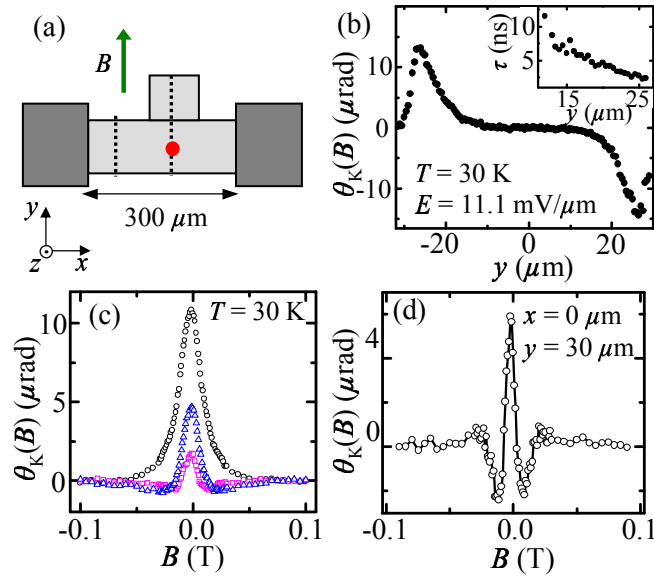


## Figure captions

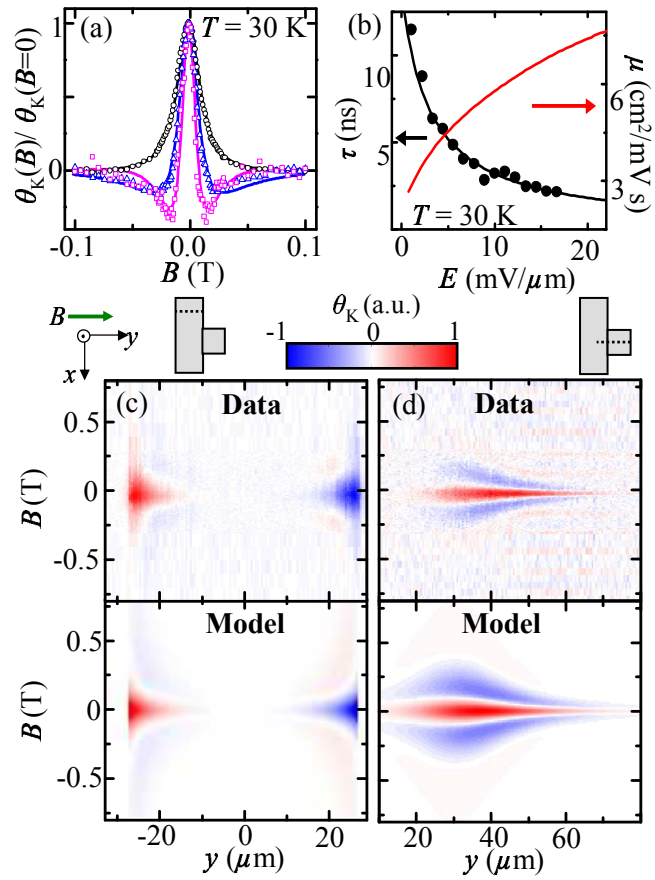
Figure 1. (a) Schematic of the 60- $\mu\text{m}$  wide channel with a transverse arm. The origin is defined to be at the center of the transverse arm in  $x$  and at the center of the main channel along  $y$  (red dot), and the dotted lines represent the location of scans discussed in the text. (b)  $\theta_K(B)$  taken away from the transverse arm for  $x \approx 50\mu\text{m}$  and  $y = -26\mu\text{m}$  (black circles),  $-22\mu\text{m}$  (black circles), and  $-18\mu\text{m}$  (magenta squares). (c)  $s^z(y)$  for  $B = 0$  away from the transverse arm ( $x \approx 50\mu\text{m}$ ). The inset shows the spin coherence time  $\tau(y)$  extracted by assuming a Lorentzian lineshape in the Hanle model. (d) Characteristic  $\theta_K(B)$  data from the center of the transverse arm at  $x = 0$ . The line is a guide to the eye.

Figure 2. (a) Normalized  $\theta_K(B)$  from Fig. 1c, corresponding to data near the channel edge,  $\sim L_s$  from the edge, and  $\sim 2L_s$  from the edge. Lines are calculations from the diffusion model described in the text. (b)  $\tau(E)$  and  $\mu(E)$  used in the model calculations.  $\tau$  is obtained from  $s^z(B)$  scans near the channel edge for various  $E$ , while  $\mu(E)$  comes from measurements on a Hall bar. (c) Data is an image  $\theta_K(B, y)$  along the main channel width clearly showing the decreasing central peak width away from channel edge and sign change away from the central peak. The lower panel shows model calculations of  $s^z(B, y)$  as discussed in the text. (d) Data is an image  $\theta_K(B, y)$  at  $x = 0$  in the transverse arm showing the complicated spin accumulation profile. The lower panel shows diffusion model calculations of  $s^z(B, y)$  as discussed in the text.

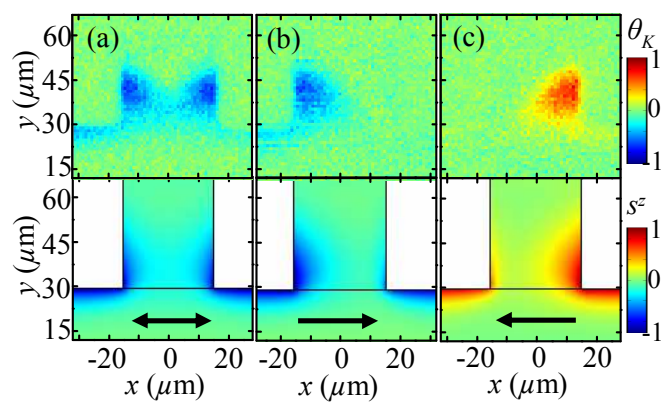
Figure3. Images of  $\theta_K$  and calculated  $s^z(B = 0)$  in the transverse arm. The top panels are data and the bottom panels are model calculations as described in the text. The electric field in the channel has magnitude  $E = 11.1\text{mV}/\mu\text{m}$  along  $\hat{x}$ , and is applied as (a) a square wave, (b) an offset square wave between 0 and  $E$ , (c) an offset square wave between 0 and  $-E$ . Data is normalized to the peak values for part (a).



Stern, *et al.*  
Fig. 1



Stern, *et al.*  
Fig. 2



Stern, *et al.*  
Fig. 3